Dual Carrier Investigations at the Mars Deep Space Station

S. S. Kent
R. F. Systems Development Section

Dual carrier transmission from a deep space station can result in receive-band interference signals. Investigations have been conducted at the Mars Deep Space Station to determine the impact of this interference on telemetry and doppler data in terms of the carrier-to-interference power ratio. These investigations were limited to uncoded data at 2048 bits/s and to a fixed (near zero) doppler frequency.

In general, it is seen that for carrier loop margins near 20 dB (typical of Viking orbital operations), the presence of detectable receive-band intermodulation interference will produce detectable data degradation.

I. Introduction

Receive-band interference resulting from high power diplexing with dual carrier uplink has been discussed in two previous reports (Refs. 1, 2). Previous investigations were primarily concerned with locating the sources and determining the signature of the interfering signals along with reduction of the level of the interference. This report will show, to some extent, the possible effect of the interference on telemetry and doppler data.

Two types of dual carrier interference were investigated (Ref. 2): (1) broadband noise bursts that occur in conjunction with intermodulation products (IMPs) and, (2) IMPs with negligible noise bursts. The first type of interference was achieved by irradiating the antenna surface, while the second type was achieved by transmitting into a water load located in the S-Band Polarization Diversity (SPD) feed cone at the antenna port of the diplexer.

II. Instrumentation for Interference

In order to characterize the interference so as to correlate it with the anticipated data degradation, the following instrumentation systems or assemblies were employed:

(1) Open-loop T_{op} instrumentation[1]

[1]This instrumentation actually measured $GkT_{op}B$ as a function of time where

G = total receiver gain to the detector
k = Boltzmann's constant
T_{op} = system operating temperature in kelvins
B = equivalent RF noise bandwidth of the detector

(2) Receiver No. 1 operating in narrow-band loop and narrow-band automatic gain control (AGC) modes

(3) Dual channel strip chart recorder for recording T_{op} and receiver No. 1 AGC voltage.

The T_{op} instrumentation was operated in the 1-MHz bandwidth mode with its output recorded on one channel of the strip chart recorder with receiver AGC voltage on the other. Channel 1 afforded a permanent recording of all noise burst activity of duration greater than 0.1 s (approximately). Typically the strip chart recorder was operated at a speed of 1.27 cm (0.5 in.)/min and was calibrated for 100 K full scale for antenna operation or 500 K for water load operation.

Channel 2 of the recorder was calibrated from -130 to -170 dBmW in terms of receiver 1 AGC voltage. Thus, any IMP sufficient to enable the receiver to acquire lock was characterized in terms of its mean and variance directly as related in time to the noise burst activity. Since the intent of the testing was to determine actual data degradation, the normal station configurations for on-site systems testing were employed. Operational test software was also used to facilitate use of station equipment and personnel. The telemetry system was tested in accordance with portions of TP 853-30/2A-04 while the doppler system was tested in accordance with TP 853-32/2B-08.

III. Test Description

In order to evaluate the effects of IMPs/noise bursts on the data, it was decided that three primary test modes would be satisfactory: (I) IMP frequency (Ref. 2) coinciding exactly with the simulated spacecraft carrier frequency; (II) IMP frequency coinciding exactly with the spacecraft subcarrier frequency; and (III) IMP frequency half-way between the spacecraft carrier and subcarrier frequencies. Other modes could be tested, but it was felt that III would be the typical case and I and II would be worst cases.

Figure 1 is a block diagram of the configuration employed to enable testing for telemetry and doppler data degradation simultaneously. It should be noted that receiver No. 1 received only the IMP/noise burst signal whereas receiver No. 2 received the test signal plus the IMP/noise burst signal. Also, the synthesizer/Iso Amp/$\times 3$ combination is required to enable doppler extraction within the usable bandwidth limits of the doppler extractor assembly.

The data outputs from this configuration are:

(1) Strip chart recorder:
  (a) T_{op}
  (b) IMP level, AGC in dBmW

(2) Bit error rate (BER)

(3) Doppler phase jitter, in deg rms (σ)

Time was recorded on the various data records so as to enable correlation of the data in terms of IMP/noise burst levels and BER or σ.

All the data discussed herein was obtained while transmitting on channels 6 and 23 and receiving on channel 17. These channels were deliberately chosen to produce an $N = 31$ (Ref. 2) interference signal which, in turn, creates the strongest IMP/NB levels for the channel crystallization available at the site (see Fig. 1 of Ref. 2 for IMP level versus N).

Table 1 is a listing of the various frequencies required in order to achieve operation in Modes I, II, and III. Note that each of the frequencies is tabulated as a VHF frequency—this is done because (1) all voltage-controlled oscillators (VCOs) are counted at this frequency, and, more importantly, (2) this enables achieving the frequency accuracies required to conduct the tests.

Due to the shortage of station time available for these tests (one 8-hour block per week), some of the doppler and telemetry testing had to be conducted simultaneously which somewhat restricted data taking for doppler degradation determination; i.e., when ST_B/N_o is set for telemetry, the margin (signal-to-noise ratio) for doppler becomes a dependent variable for any given modulation index. For these tests, the values of ST_B/N_o used were 3, 6, and 10 dB. These values resulted in doppler margins of 17, 20, and 24 dB, respectively.

Subsequent to the start of these tests, an IMP generator (Ref. 4) was developed as an aid in dual carrier investigations. Tests at the Venus Station (DSS 13) have demonstrated that the IMP generator is equivalent to an internal source (waveguide component) of IMPs in both amplitude and phase signature. It doesn't, however, simulate the noise burst signature encountered on the antenna surface. This generator was used to facilitate doppler data gathering in a more orderly and controllable manner.

As shown in Fig. 1, the IMP generator was connected in series with the water load for the doppler testing.

Thus, whenever operating into the water load, it was possible to control the level of the simulated IMPs from −120 dBm to well below receiver threshold (« − 174 dBmW).

IV. Telemetry Test Results

For all telemetry data, the bit rate was 2048 bps uncoded and the modulation index gave 8 dB carrier suppression. Figures 2 through 4 show the results of IMP/noise burst interference for each of the modes of operation tested.

Figure 2 is the result of transmitting the dual carrier signals into the water load. The interfering signal in this case consisted of IMPs with negligible noise bursts. Figure 3 is the result of irradiating the antenna surface with the dual carrier signals. The interfering signal in this case consisted of IMPs in conjunction with considerable noise bursts. Comparison of Figs. 2 and 3 shows that the presence of noise burst activity degrades the data significantly. The two probable reasons for the increased degradation are (1) increased variance of the IMP, and (2) increase in T_{op} during noise burst activity (Ref. 2).

Figure 4 shows the Mode II (IMP on subcarrier) operation degradation resulting from transmitting dual carriers into the water load. Comparison of Figs. 2 and 4 indicates that Mode I is more sensitive to IMP/noise burst interference. At this writing no attempt has been made to model the degradations measured to date.

Some attempts were made to gather data in the Mode III configuration, but time limitations generally precluded gathering of any really significant data. Scattered data points indicate, however, that Mode III is the least sensitive to IMPs/noise bursts, as would be expected.

V. Doppler Test Results[2]

A. General

Figures 5 through 9 show doppler degradation resulting from each of the modes tested. Data for Figs. 6, 7, and 8 were gathered through the use of the IMP generator. Figure 9 represents data resulting from irradiating the antenna surface with either dual 40-kW or single 400-kW carrier signals.

B. Model

An attempt was made to model the degradation for noise burst-free Mode I operations by assuming that the IMP spectrum is noise-like and constant over the receiver loop bandwidth, $2\beta_L$. The loop margin can be written as

$$m = \frac{P_c}{N_o 2\beta_{L_o}} \tag{1}$$

where

P_c = carrier power level

N_o = noise spectral density (one sided)

β_{L_o} = design point loop bandwidth (one sided)

The signal-to-noise ratio in the actual two-sided loop bandwidth, $2\beta_L$, is

$$\text{SNR} = \frac{P_c}{N_o 2\beta_L} \tag{2}$$

From Eq. (1) this can be rewritten as

$$\text{SNR} = m\frac{\beta_{L_o}}{\beta_L} \tag{3}$$

Defining the signal-to-IMP ratio as

$$\text{SIR} = \frac{P_c}{P_I} \tag{4}$$

and applying the factor β_{L_o}/β_L, an effective IMP margin, m_I, can be derived as

$$m_I = \frac{P_c}{P_I} \cdot \frac{\beta_L}{\beta_{L_o}} \tag{5}$$

Thus, the carrier to IMP ratio can be related in terms of loop margin. The total variance σ^2 of loop phase noise should then be the sum of the two individual variances, or

$$\sigma_T^2 = \sigma_m^2 + \sigma_{m_I}^2 \tag{6}$$

Equation (6) is plotted in Fig. 7 for P_c/P_I ratios of +5, +10, +20 and $+\infty$ dB.

The data points plotted on Fig. 7 represent those in which no cycle slippages occurred. Except for two points,

[2]All of the doppler phase jitter data is compared against Fig. 9 of the theoretical doppler model established by J. R. Lesh in Ref. 3.

the data are in good agreement with the simple model assumed.

It should be noted that Fig. 6 includes data points that had cycle slippage occur (the circled number indicates the number of cycles slipped). These points do not fit with the model derived as evidenced by a comparison with Fig. 7.

C. Cycle Slippage

Theory predicts large phase variance as the loop margin approaches 0 dB. This is indeed true to the point where cycle slippage actually occurs. The simple model used herein also predicts the same behavior as P_I approaches P_c, which also proved to be the case from actual tests. The test program counts the slipped cycles and gives a printout. Fig. 8 is a plot showing cycle slippage as a function of both loop margin m and P_c/P_I ratio.

D. Antenna Irradiation

Figure 9 is the phase jitter resulting from radiating dual 40-kW or single 400-kW carriers from the antenna. In the case of the dual 40-kW carriers, all data points except one had some cycle slippage occur during the averaging time. The computer program does not include cycle slippage in its calculations of phase variance so that the resultant variances are subject to considerable question as to validity. During this period of time, the noise burst activity could best be described as moderate in terms of frequency of occurrence, with T_{op} peak amplitudes of 29 K compared to a steady-state level of 22 K. The IMP variance for these data was as much as ± 12 dB as opposed to the usual 1 to 2 dB variance of the IMP generator.

The single carrier data indicates that light to moderate noise burst activity has no apparent effect on the doppler quality. The noise burst activity relating to the single carrier data points of Fig. 9 gave T_{op} amplitude peaks varying from 23 to 29 K (over a steady-state level of 22 K) and varying in occurrence from once to five times a minute.

VI. Conclusions

From the results of testing to date, it can be concluded that:

(1) Data degradation is directly related to the amount of IMP/noise burst activity.

(2) Data quality is most sensitive to IMPs interfering with the carrier signal.

(3) In the case of telemetry, some degradation does occur where IMPs interfere with the subcarrier.

(4) IMP activity sufficiently removed from both the carrier and subcarrier does not affect the data quality.

(5) Noise burst activity, by itself, is less detrimental to data quality than is combined IMP/noise burst.

(6) Measurable degradation of bit error rate and doppler jitter occur whenever the carrier to mean IMP ratio is 20 dB or less, but only if it occurs on or near the carrier or subcarrier frequencies.

(7) Even large noise burst activity ($\Delta T_{op} \sim 100$ K) does not completely destroy data under typical operating signal level margins.

References

1. Bathker, D. A., and Brown, D. W., "Dual Carrier Preparations for Viking," in *The Deep Space Network Progress Report,* Technical Report 32-1526, Vol. XIV, pp. 178–199. Jet Propulsion Laboratory, Pasadena, Calif., April 15, 1973.

2. Bathker, D. A., and Brown, D. W., "Dual Carrier Preparations for Viking," in *The Deep Space Network Progress Report,* Technical Report 32-1526, Vol. XI, pp. 146–149. Jet Propulsion Laboratory, Pasadena, Calif., Oct. 15, 1972.

3. Lesh, J. R., "Theoretical Analysis of the Doppler System Test," in *The Deep Space Network,* Technical Report 32-1526, Vol. XV, pp. 190–202. Jet Propulsion Laboratory, Pasadena, Calif., June 15, 1973.

4. Kolbly, R. B., "Intermodulation Products Generator," in *The Deep Space Network Progress Report,* Technical Report 32-1526, Vol. XV, Jet Propulsion Laboratory, Pasadena, Calif., June 15, 1973.

Table 1. Frequency predicts for data degradation tests

Mode	Exciter 1	Exciter 2	Receiver 1	Receiver 2	Test transmitter	Ext. synthesizer
I	22045604.00	21985251.00	23395713	23395713	19133237.60	22023153.70
II	22045604.00	21985251.00	23395713	23398214	19135237.60	22025455.78
III	22045604.00	21985251.00	23395713	23396964	19134237.60	22024304.74

All frequencies are in hertz.
Subcarrier frequency = 240,000 Hz.
Data rate = 2048 bits/s, uncoded.

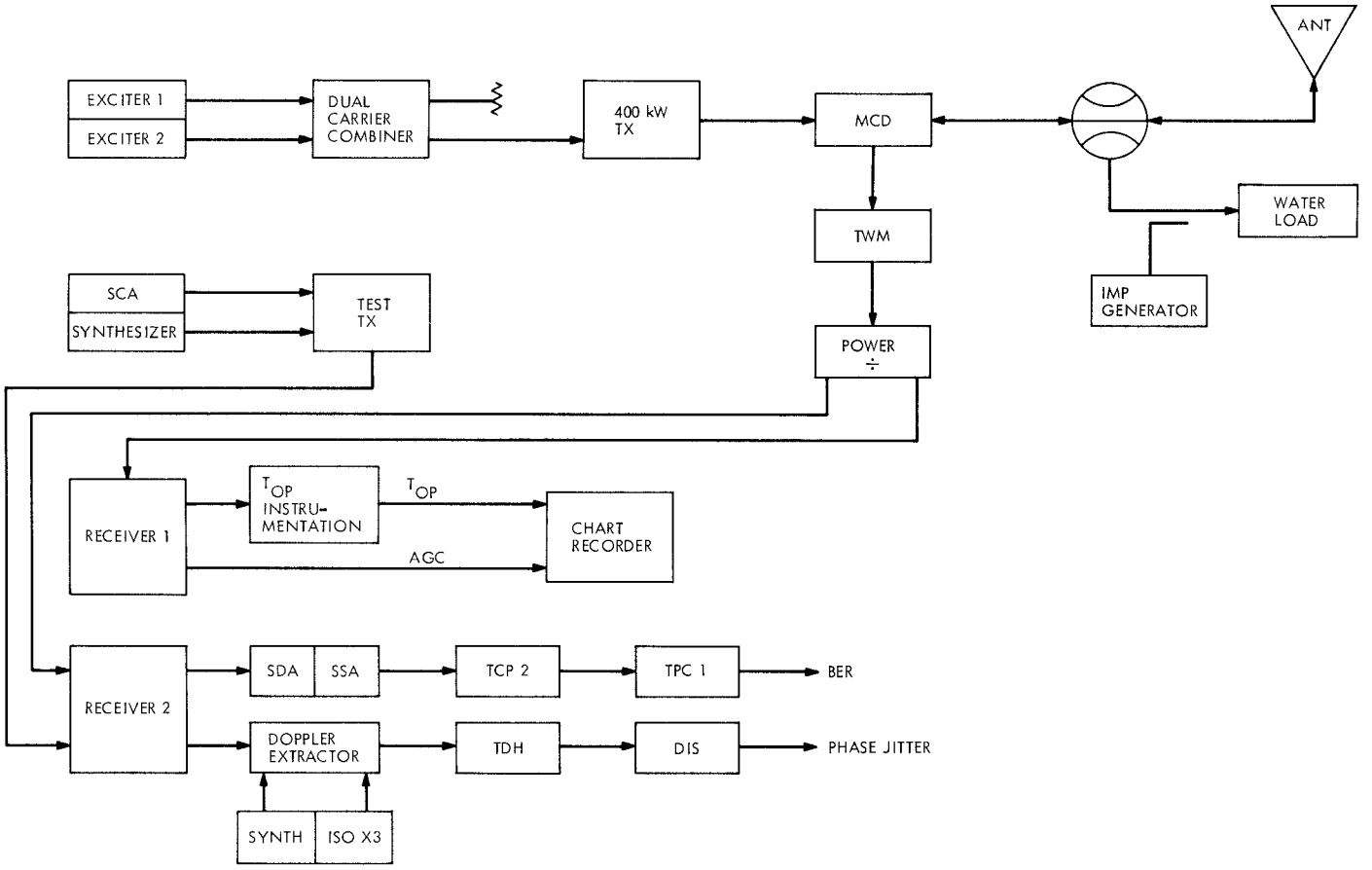

Fig. 1. Block diagram of DSS 14 dual carrier tests

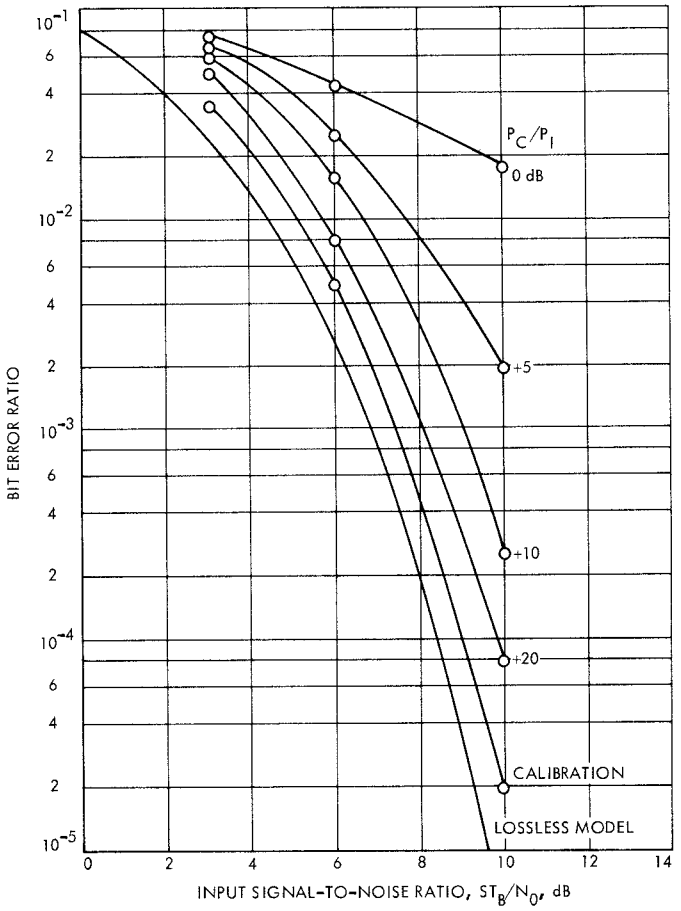

Fig. 2. Telemetry bit error rate as a function of carrier to mean IMP power ratio, Mode I operation. Cone water load configuration

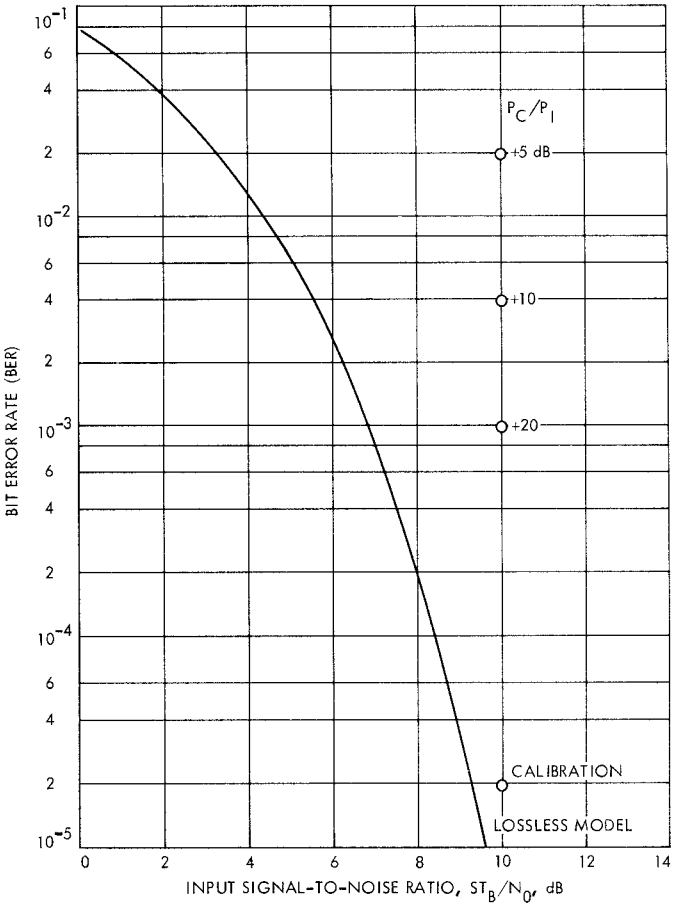

Fig. 3. Telemetry bit error rate as a function of carrier to mean IMP power ratio, Mode I operation. Antenna configuration

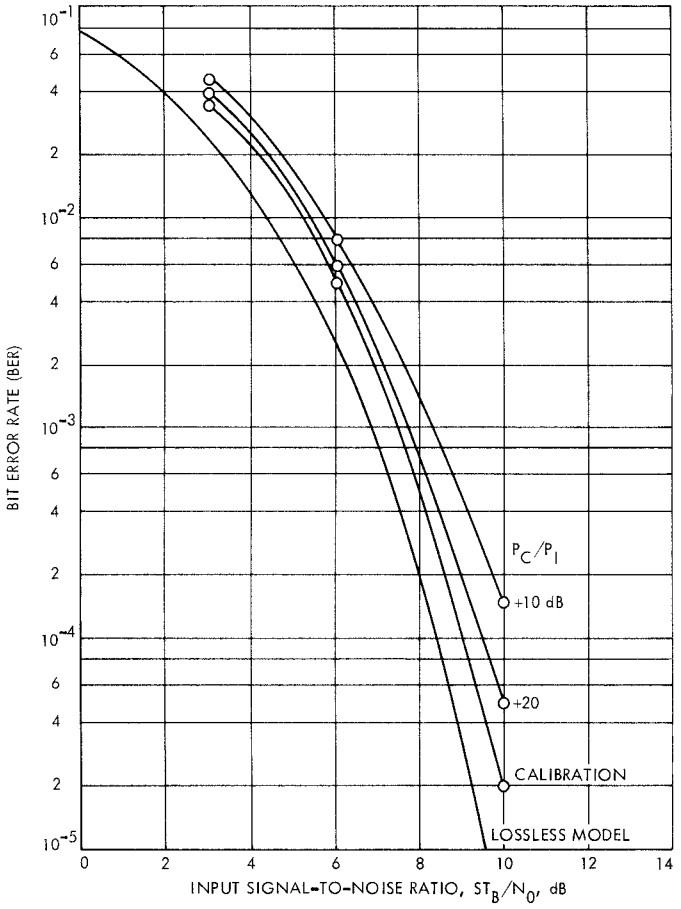

Fig. 4. Telemetry bit error rate as a function of carrier to mean IMP power ratio, Mode II operation. SPD cone water load configuration

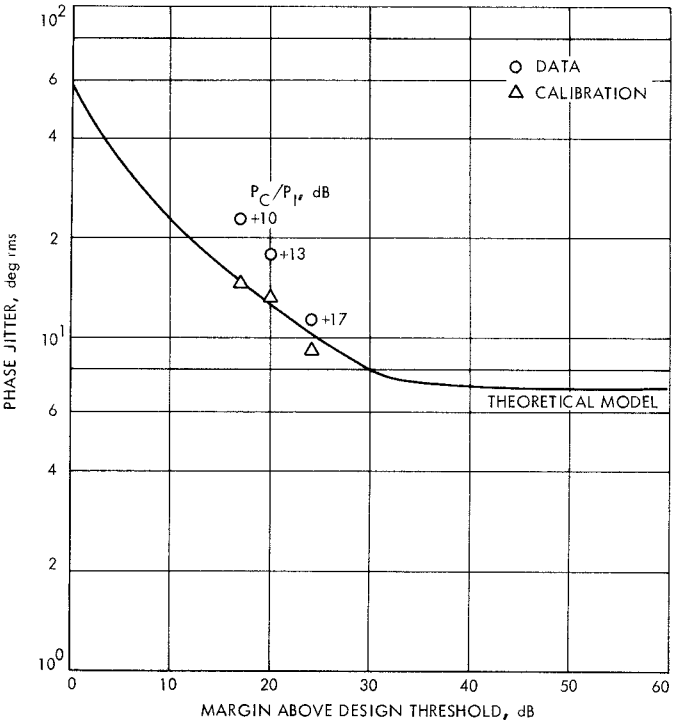

Fig. 5. Doppler phase jitter as a function of carrier to mean IMP power ratio. SPD cone water load configuration

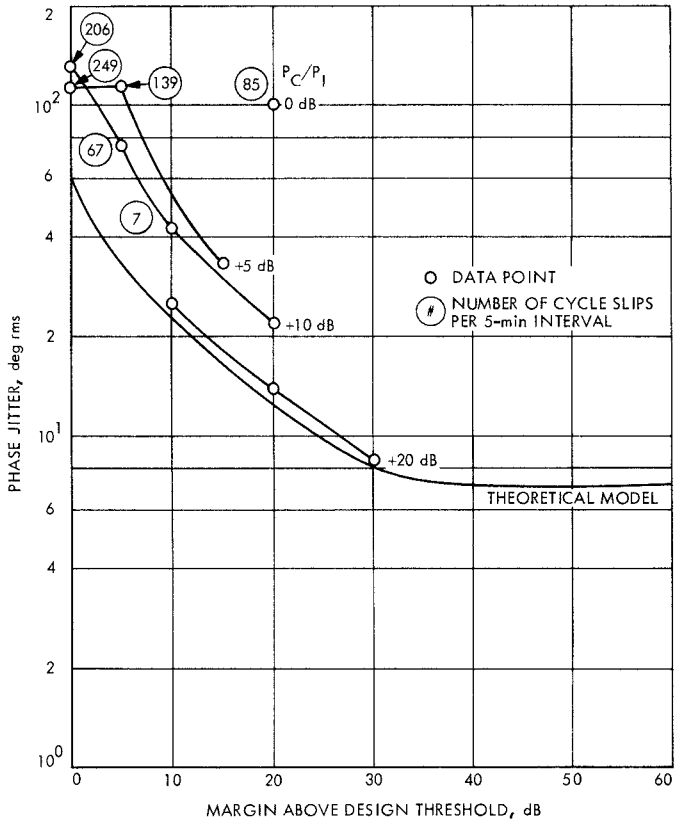

Fig. 6. Doppler phase jitter as a function of carrier to mean IMP power ratio, Mode I operation. SPD cone water load/IMP generator configuration

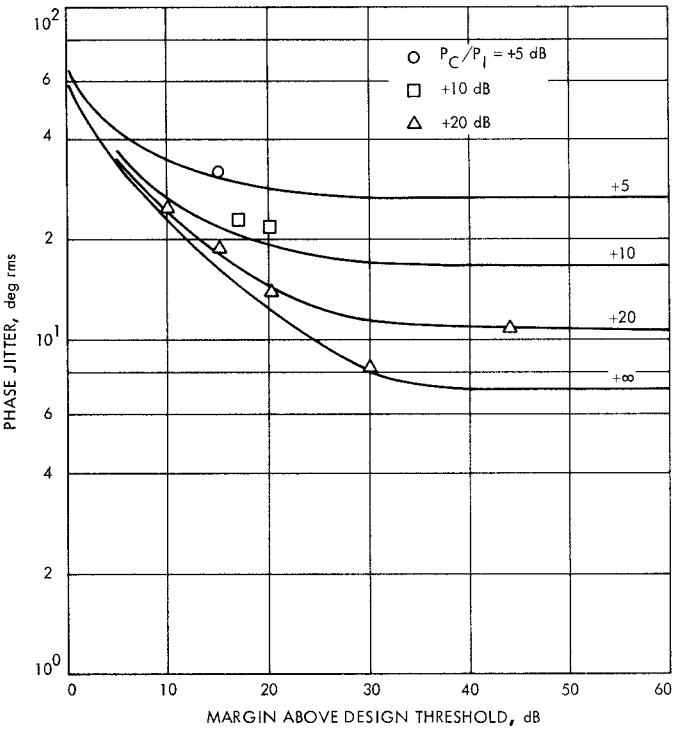

Fig. 7. Mathematical model vs actual doppler phase jitter as a function of carrier to mean IMP power ratio, Mode I operation. SPD cone water load/IMP generator configuration

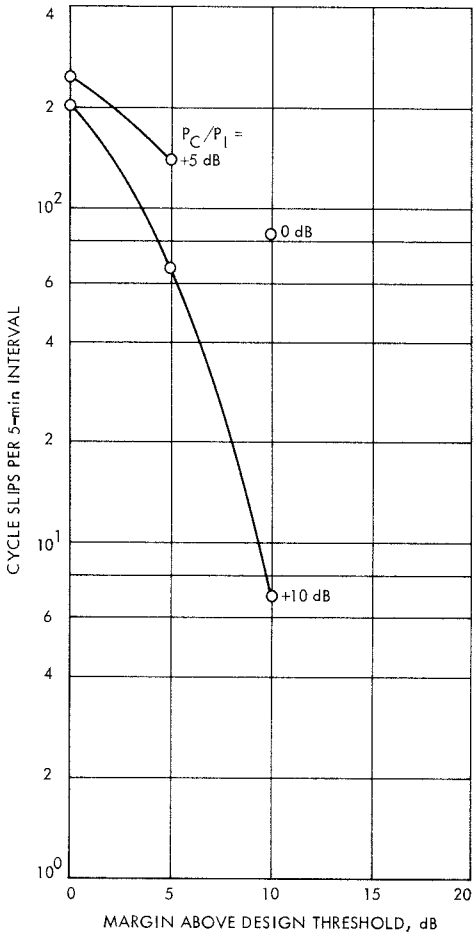

Fig. 8. Doppler cycle slips as a function of carrier to mean IMP power ratio, Mode I operation. SPD cone water load/IMP generator configuration

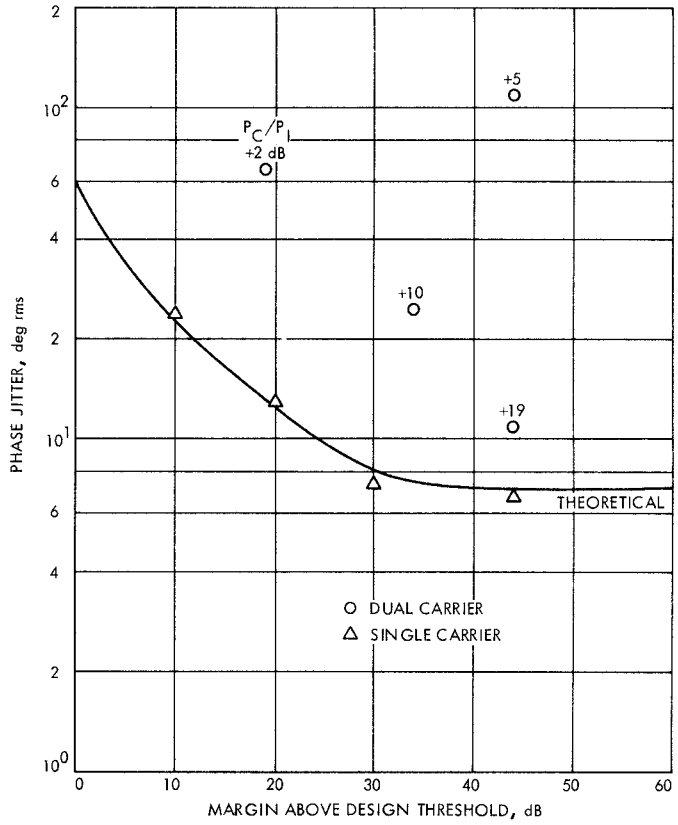

Fig. 9. Doppler phase jitter as a function of carrier to mean IMP power ratio, Mode I operation. Antenna configuration